Search for spin-polarization effects in $La_{0.7}Mn_{0.3}Ca_3O_3/YBa_2Cu_3O_{7-\delta}$ thin-film bilayers

X. Deng,[1] M. Joshi,[1] R. Chakalova,[1] M. S. Colclough,[1] R. Palai,[1,3,*] Y. Y. Tse,[2] I. P. Jones,[2] H. Huhtinen,[1,4,†] and C. M. Muirhead[1]

[1]*School of Physics and Astronomy, University of Birmingham, Edgbaston, Birmingham B15 2TT, United Kingdom*

[2]*School of Engineering, University of Birmingham, Edgbaston, Birmingham B15 2TT, United Kingdom*

[3]*Department of Physics, University of Puerto Rico, San Juan, Puerto Rico 00931-3343, USA*

[4]*Department of Physics, University of Turku, Turku FIN-20014, Finland*

(Received 6 November 2007; revised manuscript received 9 March 2008; published 30 April 2008)

We describe a search for the effects of spin-polarized electrons in thin-film bilayers consisting of the high temperature superconductor $YBa_2Cu_3O_{7-\delta}$ and the colossal magnetoresistive material $La_{0.7}Ca_{0.3}MnO_3$ by using penetration depth and critical current measurements. The work differs from that described in other works in that the $YBa_2Cu_3O_{7-\delta}$ is grown with its *c*-axis lying in the plane of the thin film in order to investigate the effects of proximity suppression and also the injection of a spin-polarized current along the *a*/*b*-planes of the $YBa_2Cu_3O_{7-\delta}$. We see a number of effects including field dependence of the average penetration depth and apparent suppression of the critical current by an injected current, with a gain greater than unity, but we argue that these are explicable in terms of a combination of heating and current summation, without any need to invoke the spin–polarization of the injected current.

DOI: 10.1103/PhysRevB.77.144528 PACS number(s): 75.70.Cn, 91.60.Pn

I. INTRODUCTION

There are two basic types of experiment that probe the effect of ferromagnetic layers on superconducting thin films: (i) those which measure the equilibrium state of the system and are, in essence, studies of the proximity effect, and (ii) nonequilibrium effects, which involve current injection from the ferromagnet into the superconductor at energies above the gap. Suppression of superconductivity is then expected when either the proximity coupling length or the spin-diffusion length in the superconductor becomes significant compared to the film thickness.

There have now been a number of papers claiming to observe the effect of the injection of spin-polarized electrons on the superconducting state of high temperature superconductors (HTSs),[1–11] although the validity of much of the literature has been challenged.[12] In most studies the critical current (I_C) is suppressed by an injection current (I_{inj}), and in some cases a gain $G=-\Delta I_C/I_{inj}$ greater than unity has been claimed, with a maximum of 35 for injection from $La_{0.7}Sr_{0.3}MnO_3$ (LSMO) into $YBa_2Cu_3O_{7-\delta}$ (YBCO).[10] If this is indeed caused by the effect of spin-polarized injection, then it is likely to be a fast process and opens the way for useful devices. It is also of fundamental interest because of the light it may throw on the superconducting state in HTS and, in particular, the question of spin-charge separation.[13,14]

A number of structures and materials have been employed for these measurements. Some have used conventional metals as the ferromagnet,[9,11] but most have used a colossal magnetoresistance material such as $La_{0.7}Ca_{0.3}MnO_3$ (LCMO) or LSMO because these are believed to be almost 100% spin–polarized, and because they epitaxially grow onto YBCO under very similar growth conditions, leading to interfaces which are sharp on the atomic scale.

The potential problem due to heating by the injection current has been recognized by a number of authors[2–4,12] and in some cases, pulsed currents have been used to minimize the effect.[4,15] Unfortunately, this only precludes heating of the substrate: thermal relaxation between the HTS film and the substrate may only take a few tens of nanosecond,[16] and pulsed measurements on a time scale short enough to preclude this possibility have not been reported.

In a number of works, an applied magnetic field has been used to take the ferromagnet around its hysteresis loop. In most cases, it has been found that the superconducting state is less suppressed close to the coercive field than when the ferromagnet is near saturation, and this has been used as evidence of the effect of the spin-polarized state of the ferromagnet on the superconducting order parameter.[9,17,18] The argument is that suppression of superconductivity due to spin–polarization is expected to be strong where the magnetization in the ferromagnetic layer is large. In the vicinity of a magnetic domain wall, we could expect partial cancellation of any suppression, the extent of the cancellation depending on the characteristic lengths for spin diffusion and proximity coupling, and the density of domain walls, which is near maximal at the coercive field. This effect has been reported in *c*-axis perpendicular-to-plane LCMO/YBCO films for both mutual inductance[17] and critical current measurements[18] and in the critical current of niobium/cobalt layers.[9] In all the cases, the effect is small. In Ref. 17, the effect was removed when a 1 nm layer of $SrTiO_3$ (STO) was inserted between the LCMO and YBCO layers, confirming that the suppression was due to an electronic interaction rather than the direct effect of the magnetic field. Experiments have also been reported in trilayer spin-valve structures (*F*/*S*/*F*) for both LCMO/YBCO/LCMO (Refs. 19 and 20) and conventional ferromagnet/superconductors[21] with both magnetic field and current in plane. In Ref. 19, there was *maximal* suppression of superconductivity at the coercive field, although in this case, it was interpreted as being associated with antiparallel alignment of the two LCMO layers close to the coercive field. It was argued that this resulted in additional pair breaking effects in the YBCO layer caused by trapping of polarized spins scattered into the YBCO from the ferromagnetic layers. Direct effects due to magnetic fields were precluded on the grounds that the effects were absent in YBCO/LCMO bilayers. Reference 20, however, reported exactly opposite

effects, with maximal suppression of superconductivity when there was *parallel* alignment of the ferromagnetic layers. Again, the effects were attributed to an additional pair breaking effect arising from spin imbalance in the superconducting layer. Reference 21 also observed suppression of superconductivity close to the coercive field but interpreted this as a direct result of flux flow due to magnetic fields penetrating the superconductor at the Bloch domain wall boundaries. The enhanced effect in the trilayer structures resulted from a cooperative alignment of the magnetic domains on opposite sides of the *S* layer. In this model, there was therefore no need to assume any additional proximity or pair breaking effects in the *S* layer.

A number of geometries have been used for polarized spin-injection experiments, and most of these implicitly assume that the current is injected in the *c*-direction, although some injection along the a/b-plane cannot be ruled out because of interface roughness. There has been only one reported case of deliberate injection into the a/b-plane through a ramp junction,[8] and this implied a spin-diffusion length of $\sim$1 mm, although to our knowledge, this result has not been confirmed. All superconducting properties in HTS are anisotropic, so one would be surprised if this were not also true of the spin-diffusion length. There is particular interest in structures where the ferromagnet faces the HTS at 45° to the *a* and *b*-directions since it is well established that there are nodes in the energy gap of YBCO in this direction. This means that it should be easier to inject spin-polarized quasiparticles at low energy, and that thermally excited quasiparticles may have a significant effect on the superconducting state of the HTS even in the absence of an injected current. As noted above, effects due to spin-polarized quasiparticles will be substantial when the proximity coupling length or the spin-diffusion length becomes comparable to the film thickness. The most sensitive measurements should therefore be in thin-film HTS/ferromagnet bilayers grown with the *c*-axis in plane and with the node in the energy gap perpendicular to the interface with the ferromagnet.

In this paper, we report measurements of the average penetration depth via mutual inductance measurements through such an LCMO/YBCO bilayer in the equilibrium state and also the nonequilibrium effect of spin-polarized injection via measurement of the critical current. We describe the measurements in some detail because such detail is lacking in much of the literature.

II. EXPERIMENTAL METHOD

A. Film growth and characterization

In Fig. 1, we show the *c*-axis in-plane growth of our films compared to the *c*-axis perpendicular growth used in other reported works on spin–injection into HTS films. All the films used in our experiments were grown by using pulsed laser deposition (PLD). The YBCO and LCMO layers were both 100 nm thick, grown at 700 °C in an oxygen atmosphere of 0.7 mbar, and annealed in 0.8 bar of oxygen for 20 min at 500 °C before being allowed to naturally cool. Those for mutual inductance measurements were grown on STO substrates. Although the (110) surface of the substrate

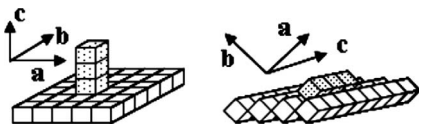

FIG. 1. The usual *c*-axis perpendicular-to-plane growth of YBCO on a (100) polished substrate. (b) the *c*-axis in-plane growth of YBCO on the (110) polished substrates used in our experiments. The subsequent LCMO layer grows with the same orientation and has a pseudocubic unit cell

strongly encourages *c*-axis in-plane growth of the YBCO, along with other authors,[22,23] we find that in order to obtain a good epitaxial *c*-axis in-plane growth of the YBCO layer, and hence of the subsequent LCMO layer, it is necessary to grow a thin buffer layer. For STO substrates, PBCO (30 nm grown at 600 °C and 0.2 mbar oxygen) provides a good solution, with lattice parameters intermediate between those of YBCO and STO. All the layers in these films were grown *in situ*.

The films used for the critical current measurements were grown on $La_{0.3}Sr_{0.7}Al_{0.65}Ta_{0.35}O_3$ (LSAT) substrates. Here, the lattice match between YBCO and LSAT is much better than that between YBCO and STO, and a buffer layer of YBCO (50 nm deposited at 600 °C and 0.2 mbar of oxygen) is sufficient to obtain an almost 100% *c*-axis in-plane growth. The LCMO layer for these films was deposited after a patterning process (see Sec. II C below).

X-ray diffraction (XRD) measurements were performed with a Bruker-Siemens D5000 four-circle diffractometer fitted with two additional orthogonal arcs for sample alignment. θ-2θ, χ, ω, and ϕ scans were used to verify the true *c*-axis in-plane growth of the YBCO and epitaxial growth of the LCMO layer. Transmission electron microscopy (TEM) measurements were made using a Tecnai F20 fitted with an energy dispersive x-ray spectroscopy (EDX). This was used to obtain images and for high resolution chemical analysis.

Temperature dependent measurements of the electronic properties were made in a continuous flow cryostat. A magnetic field up to 150 mT was applied in both the mutual inductance and critical current measurements. The field was applied in the plane of the film, which is either parallel or perpendicular to the YCBO *c*-axis, or applied perpendicular to the film surface. In order to provide a field of high uniformity, the room temperature electromagnet was fitted with special pole pieces. We discuss the need for field uniformity in Sec. III B. M/H and M/T measurements for our samples were made with a commercial superconducting quantum interference device magnetometer.

B. Mutual inductance measurements

A typical measurement is shown in Fig. 2, with a schematic of the measurement system shown in the inset. The films were unpatterned and 10 mm square. Above T_C, the substrate and the deposited films have negligible effect on the mutual inductance, which is taken as its free space value M_o. As the temperature is reduced below T_C, the mutual inductance decreases as the average penetration depth λ decreases.

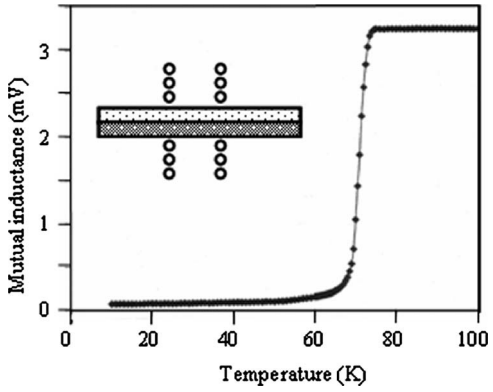

FIG. 2. A typical mutual inductance versus temperature curve. The coil geometry is shown in the inset. The upper coil is driven at 50 kHz and the lower coil is connected to a lock-in amplifier, which is set to read the signal magnitude. The coils (not to scale) are 2 mm in diameter and 1 mm thick and closely pressed against the film to reduce edge effects, particularly flux leakage around the outside of the film.

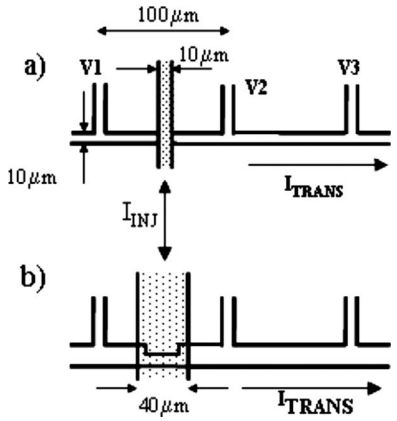

FIG. 3. YBCO tracks with voltage leads and YBCO/Au crossovers; (a) the narrow crossover and (b) the wide crossover (see text).

For sufficiently small λ, the leakage flux around the edge of the film and direct coupling between the drive and detector electronics can become significant. We have performed a separate experiment to determine the contribution from these by adding a very thin layer (0.05 mm) of lead foil cut to the 10 mm size of the substrate. Below the transition temperature of the lead (6 K), the film becomes magnetically opaque and the residual leakage signal can be determined. This was less than 30% of any of our measurements at the lowest temperature. Our measurements are therefore sensitive to changes in λ over the whole temperature range. Checks were made at various temperatures to ensure that the 50 kHz drive field was within the linear regime. In order to convert measurements of mutual inductance to average penetration depth, computer modeling is required since there is no analytical solution for finite size coils. This has been employed in our earlier reported work for *c*-axis films,[17] but since our conclusions on the (110) films will be that the observed effects are *not* due to suppression of the order parameter by polarized spins, we have not considered it worthwhile to do this here. Our mutual inductances are therefore shown as volts on the pickup coil.

C. Critical current measurements

The YBCO layer was first deposited and patterned into the required geometry for four-point measurements by using conventional UV lithography and argon-ion-beam milling. The specimen was then returned to the PLD chamber and covered with the layer of LCMO. After oxygen annealing, the sample was quickly moved into a magnetron sputtering system (base pressure of 5×10^{-8} mbar) and covered with 500 nm of gold. The sample was further patterned to provide the crossover. The final structure is shown in Fig. 3. Additional voltage leads (not shown) were added for measurement of the resistance of the gold track. Some care was required here to minimize milling into the *thickness* of the YBCO track; this was achieved by using end-point detection in the ion-beam miller. The function of the gold was to provide an equipotential layer on top of the LCMO. Ideally, this will give a uniform density for the injected current and avoid the problems of an ill-determined current transfer length that besets many other experiments.

We have used two track geometries: one has a narrow LCMO/Au crossover to give the maximum injection current density for a given total injection current and the other has a wide LCMO/Au crossover over a YBCO track with a narrowed region. This ensures that the critical current is limited by the region under the LCMO layer. We discuss this in more detail in Sec. III. For both geometries, we have patterned YBCO tracks in both the *c*-direction and *a*-*b*-direction of the YBCO in order to search for the effects of spin-polarized injection in both directions of the transport current. Both tracks were patterned with their crossovers close to the middle of the film in order to optimize the film uniformity in the two directions.

In order to avoid convolving the properties in the a/b and *c*-directions, it is necessary that the patterned tracks be accurately aligned with the a/b-planes. We have found that the principal axis for as supplied substrates can be angled by as much as 5° to the substrate edge. The alignment of all films was measured before patterning by using XRD, and corresponding adjustments were made in the mask aligner in order to ensure that the alignment of the a/b-planes was within 0.5° of the relevant patterned tracks.

III. RESULTS AND DISCUSSION

A. Sample quality

The LCMO films typically have $T_C\sim250-270$ K, which is characteristic of an optimally oxygenated material. All our YBCO samples, however, have T_C in the range 60–70 K, which is well below the (~90 K) value normally considered characteristic of high quality YBCO films. Those with an LCMO layer on top of the YBCO tend to have lower T_C values than our single layer YBCO films, although we will argue that this is not an electronic suppression of superconductivity in the YBCO by the spin-polarized electrons in the

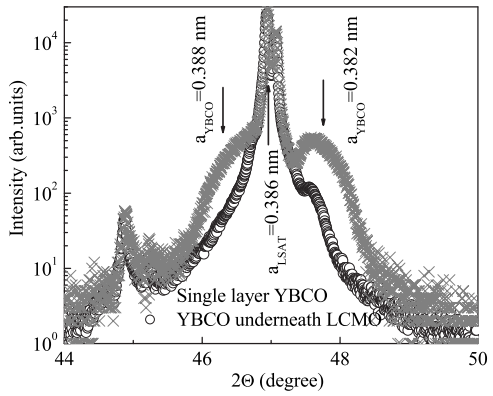

FIG. 4. Symmetric $\theta/2\theta$ scans at a tilt angle $\chi=45°$ for a 100 nm YBCO thin film on LSAT before and after deposition of the 100 nm LCMO layer.

LCMO. In contrast, we find that our PLD films grown on (100) STO or LSAT substrates, and hence with *c*-axis perpendicular to plane, all have sharp transitions in the 90 K region. A reduced T_C for *c*-axis in-plane YBCO has also been reported in the work in Ref. 24, wherein it was interpreted as due to compressive stress along the *c*-axis, which was caused by the lattice mismatch between the *c*-lattice parameter of YBCO (1.168 nm) and the cubic lattice parameter of their STO substrate (0.3905 nm).

Symmetric θ-2θ scans at a tilt angle $\chi=45°$ for one of our (110) YBCO on LSAT films before and after LCMO deposition are shown in Fig. 4. The central peak is that of the LSAT substrate. For the single layer YBCO film, the side lobes correspond to twinned YBCO with an *a*-axis with length of 0.382 nm and a *b*-axis with length of 0.388 nm, which are characteristic of a fully oxygenated, 90 K material.[25,26] In contrast to the films discussed in Ref. 24, we would not expect significant stress from our LSAT substrates. Whatever stress is present is clearly insufficient to cause an observable change in the lattice parameters. We have no explanation of the low T_C in our films, but the XRD measurements do imply that it is not a consequence of low oxygenation. This is consistent with our failure to increase the T_C of these films by postannealing in flowing oxygen. After LCMO deposition, the peaks of the *a*-axis and *b*-axis are both hidden by the central LSAT peak. The length of the *a*-axis is therefore increased, and the length of the *b*-axis is decreased compared to those before LCMO deposition, which are consistent with deoxygenation[25,26] and the further reduced T_C. A reduced T_C due to LCMO deposition has also been reported in Ref. 27 for *c*-axis perpendicular-to-plane LCMO/YBCO multilayers, wherein it was attributed to the formation of an oxygen impervious interface between the YBCO and LCMO layers.

We therefore conclude that a low T_C is characteristic of high quality *c*-axis in-plane films but that the deoxygenation and further reduction of T_C are caused by the overlying LCMO layer.

In Fig. 5, we show high resolution TEM (HRTEM) images for one of our LCMO/YBCO/PBCO/STO films. In common with many other reports on multilayer films, we see that the roughness increases as we move up through the layers. Our *c*-axis in the plane films are typically five times

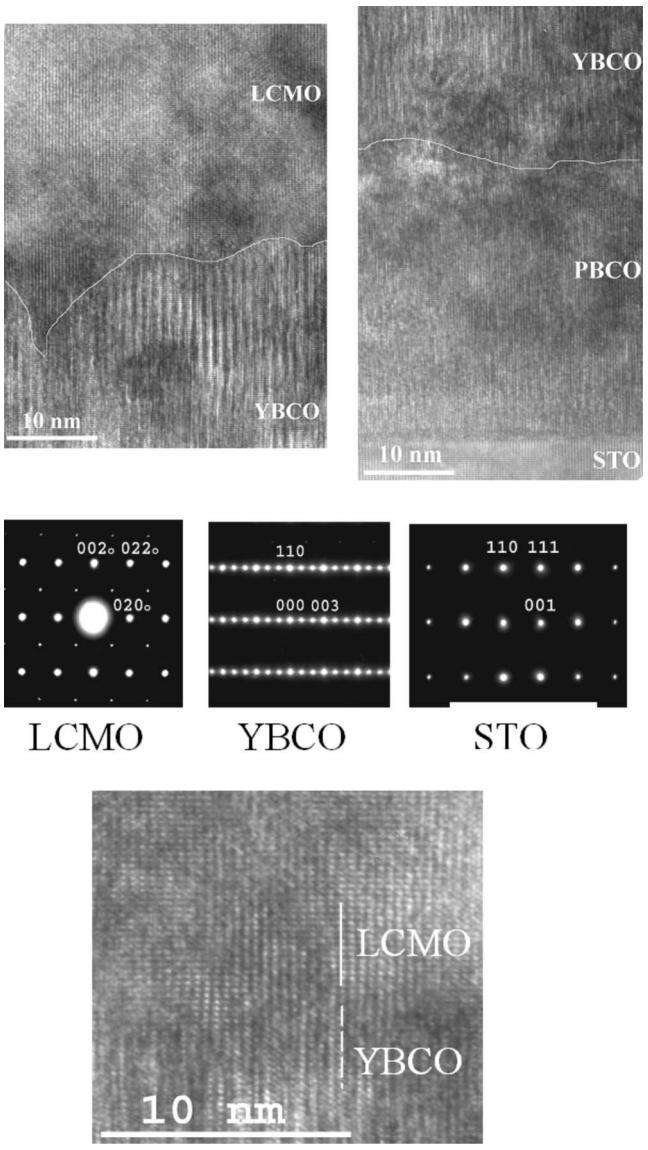

FIG. 5. A cross-sectional TEM image of a trilayer (LCMO/YBCO/PBCO) superlattice on an STO substrate; (b) the corresponding diffraction patterns along the LCMO $[100]_o$, YBCO $[\bar{1}10]$, and STO $[\bar{1}10]$ directions; (c) HRTEM showing the continuation of the (001) YBCO and (010) LCMO planes. Note that here, we have used the nomenclature for the true orthorhombic unit cell of the LCMO.

rougher than the *c*-axis perpendicular-to-plane YBCO/LCMO bilayer films grown in the same PLD system. Although the interface is not flat between each layer, the epitaxial relationship is maintained, as indicated by the continuation of the (001) YBCO to the (010) LCMO planes, as shown in Fig. 5(c). We emphasize that, although the roughness may lead to a significant injection of current into the *c*-direction, there is still a majority contact perpendicular to the substrate plane. Most importantly, our films have their thinnest dimension perpendicular to the substrate plane, so effects due to injection in the a/b-direction should be pronounced if the spin-diffusion length is significant compared to the film thickness.

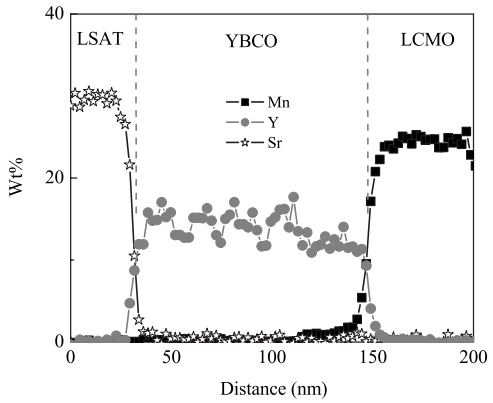

FIG. 6. Chemical profiles for strontium, copper, and manganese in an LSAT/YBCO/LCMO film. The spatial resolution is 10 nm.

In Fig. 6, we show an EDX scan across an LSAT/YBCO/LCMO film. All cations were measured, but for clarity, we show only three elements. To within the accuracy of our measurement (10 nm), we see no evidence of any cation diffusion between layers. We should note, however, that diffusion of manganese ions into the YBCO may be particularly deleterious to spin-polarized injection. We return to this point in Sec. III C.

B. Mutual inductance measurements

In Fig. 7, we show the mutual inductance and magnetization versus applied magnetic field for one of our samples and for the two different in-plane magnetic field directions.

We first note the strong anisotropy of the $M/\mu_O H$ loops, indicating a magnetically easy [100] direction in the LCMO and a harder [011] direction.

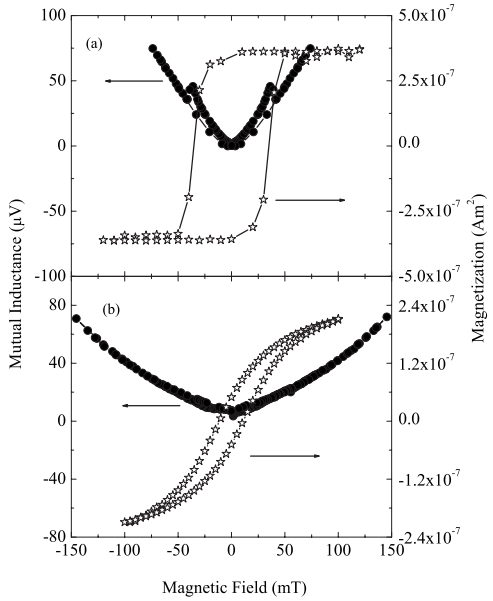

FIG. 7. Mutual inductance versus magnetic field applied in the plane of the film (sample 181) for field (a) parallel to the YBCO c-axis (LCMO [100] direction) and (b) perpendicular to the YBCO c-axis (parallel to LCMO [110] direction). T=61.3 K; T_C=64 K.

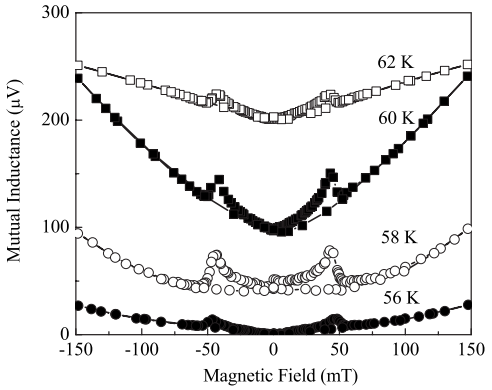

FIG. 8. Mutual inductance versus magnetic field for field parallel to the YBCO c-axis and four temperatures (sample 181). The slight reduction in peak separation with increasing temperature reflects the weak dependence of the coercive field of the LCMO on temperature. The curves have been vertically displaced for clarity.

We observe the same effect in single layer LCMO films directly grown onto (110) substrates. The anisotropy is not therefore related to the interaction with the YBCO, electronic or otherwise.

The broad quasiparabolic background to the mutual inductance is characteristic of all our measurements, and also we find it in single layer YBCO films in both c-axis in-plane and perpendicular to-plane orientations. The dependence on applied field becomes much stronger as the field direction is tilted away from the plane, tending to a linear dependence for field perpendicular to the plane. In order to minimize this effect and to make any effects due to the LCMO easier to observe, we use the high homogeneity magnet pole pieces referred to above and perform an iterative adjustment of the field angle relative to the plane, heating above T_C between each measurement.

A separate verification of the field homogeneity in the continuous flow cryostat indicates that the parabolic behavior when the field is accurately parallel to the film plane is not due to any remaining curvature of the field lines but is an intrinsic effect due to suppression of superconductivity by the applied field. A parabolic dependence on H is predicted by the Ginzburg–Landau theory.[28] We also find (Fig. 8) that the field dependence is strongest around $(0.7-0.8)T_C$, becoming progressively weaker at very low temperatures wherein superconductivity is stronger or as T approaches T_C, as expected.

The magnetic field dependence of c-axis in-plane YBCO films will be discussed in detail elsewhere.

We consider now the nonparabolic component of the mutual inductance. In Fig. 7(a), we see clear peaks in the mutual inductance for H parallel to the YBCO c-axis: these peaks closely correspond to the coercive field of the LCMO and are therefore related to the domain structure. The weak temperature dependence of the peak position reflects the weak temperature dependence of the coercive field of the LCMO below 100 K. For H perpendicular to the YBCO c-axis, however, there is no observable effect that we can relate to the magnetization. We note, however, that for perpendicular H, M changes sign over a considerably larger range in H

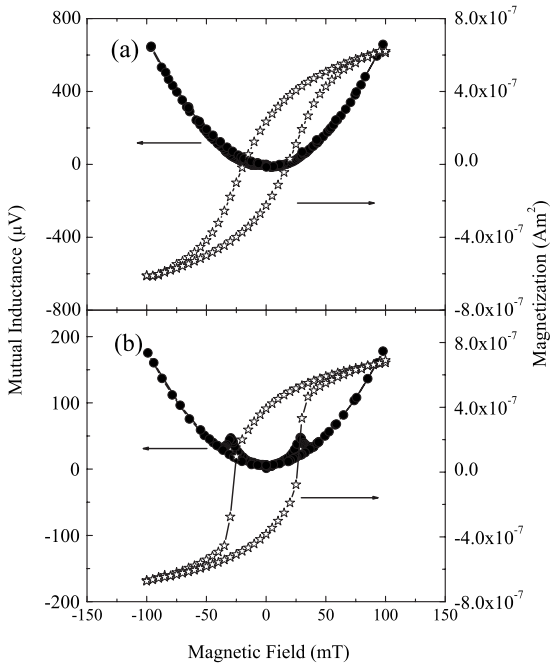

FIG. 9. Mutual inductance versus magnetic field applied in the plane of the film (sample 253). A 20 nm layer of STO inserted between the YBCO and LCMO layers has caused a reversal in the effect of the applied field (a) parallel to the YBCO *c*-axis, and (b) perpendicular to the YBCO *c*-axis, relative to the behaviour shown in Fig. 7. T=53.4 K; T_C=57.5 K.

than for parallel H, and any enhancement in the mutual inductance may well be lost in the general parabolic background. We find these strongly anisotropic effects in all the *c*-axis in-plane films that we have measured.

The important point here, however, is that we observe peaks rather than dips. Dips at the coercive field were reported in *c*-axis perpendicular-to-plane films,[17] and we find a natural explanation in the suppression of superconductivity by the LCMO, this suppression being partially relieved by the presence of magnetic domain walls, as discussed above. Peaks are therefore exactly the opposite of what we would expect if the effect were caused by suppression of superconductivity by spin–polarization in the LCMO.

As noted earlier, a key result reported in Ref. 17 was that the insertion of a thin layer of STO between the LCMO and the YBCO removed the dips, demonstrating that the dips were caused by an electronic interaction. We therefore repeated this experiment on our *c*-axis in-plane films. The result is shown in Fig. 9. We see that the overall behavior is essentially unchanged, except that the roles of perpendicular H and parallel H to the YBCO *c*-axis have been reversed. This is again a property of the LCMO growth, where the intermediate STO layer has resulted in a rotation of the magnetically easy axis from the [001] to the [011] substrate direction, which is the same as that reported for LCMO deposited on (110) $NdGaO_3$ substrates,[29] which were chosen because of their excellent lattice match to LCMO. The reduced anisotropy caused by the STO layer may reflect a reduced stress, although these effects and the different overall magnitudes are not important for our present discussion.

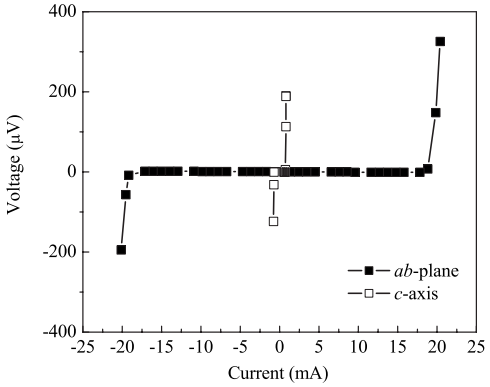

FIG. 10. V/I characteristics for sample 442 for tracks along the YBCO a/b-plane and *c*-axis directions.

Doubling the thickness of the LCMO made little difference to the observed effects, although the height of the peaks tended to be somewhat greater for thinner YBCO. We therefore attribute the peaks to a magnetic effect.

The minimum thickness $d_{\min}$ of a ferromagnet for flux penetration into an adjacent superconducting layer depends on the thickness and penetration depth of the superconductor, the saturation field of the ferromagnet and the value assumed for the width of the Bloch domain wall.[30] The data in Ref. 21 for an LCMO/YBCO bilayer gives a value for $d_{\min}$=51 nm, assuming a domain wall width of 50 nm. If we take the estimated domain wall width of 100 nm from Ref. 6, we obtain a value $d_{\min}$=25 nm. These are both below our LCMO layer thickness of 100 nm. Penetration of magnetic flux into our YBCO layer is therefore highly likely. Our model for the observed behavior is that at the domain boundaries, magnetic flux penetrates the YBCO and suppresses the average value of the order parameter, thereby increasing the mutual inductance.

In summary, we find no effect on the mutual inductance of our *c*-axis in-plane films that we can attribute to the spin-polarized nature of the LCMO.

C. Critical current measurements

Typical V/I measurements for one of our samples are shown in Fig. 10. We see that the voltage rises quasi-exponentially above I_C and is typical of flux flow resistance. The resistivity at our highest voltage is a few percent of the normal state value in both the *c* and a/b-directions. We note that the critical current is over ten times higher in the *a*-direction than in the *c*-direction, which is typical of *c*-axis in-plane YBCO films.[22,31]

Separate V/I measurements of the LCMO/Au tracks show a resistance of typically 50 mΩ/sq, whereas the vertical resistance through the crossover to the YBCO is typically 100 Ω. The current transfer length is therefore much greater than the lateral dimensions of the crossover and we are well justified in treating the Au layer as an equipotential surface. This does not, of course, prove that the injection into the YBCO is uniform nor does it tell us where the main contact resistance is other than that it is not the bulk resistance of the LCMO in the crossover, which, from separate measurements

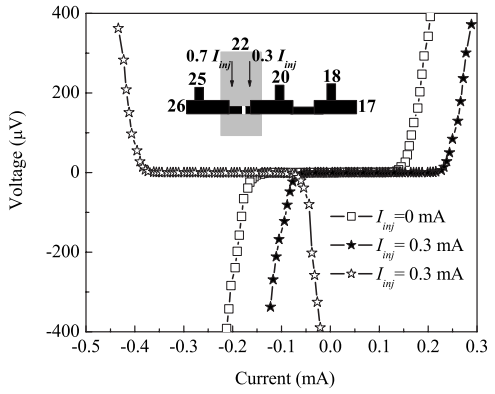

FIG. 11. Effect of current injection into sample 485 with a wide crossover. The common earth is initially at contact 26. The open squares are for $I_{\mathrm{inj}}=0$. The injection current simply causes a displacement of the V/I curves in the positive current direction (solid stars). Change of the earth connection to contact 17 causes a reversal of both the displacement direction and the voltage (open stars).

on LCMO tracks, we estimate to be ~1 mΩ. In Fig. 11, we show the effect of injection into a track with a wide crossover. We note that this sample had an anomalously low critical current in both crystallographic directions, which is presumably due to oxygen deficiency. The effect of the injected current is simply a displacement of the characteristics along the current axis due to the addition of the injected current to the transport current (I_T). It is important to note that the current axis in all our plots is derived from the measured transport current and that the injected current is separately measured, so the observed displacement is to be simply expected on grounds of current addition. The currents are determined from the voltage across small series resistors. These and the potentials between the voltage contacts are measured with high input impedance battery operated differential amplifiers. There is one common earth. Change of the common earth from contact 26 to 17 causes a reversal of both the injection current direction and the voltage. We see that the displacements in the two cases are approximately $0.7I_{\mathrm{inj}}$ and $0.3I_{\mathrm{inj}}$ implying that the critical current is limited by a region displaced from the center of the narrowed part of the track. There is, however, no significant critical current suppression for either connection nor for measurements made on a number of samples for transport current in the c-direction.

In Fig. 12, we show the effect of injection through a *narrow* crossover for transport current in the c-direction [Fig. 12(a)] and the a/b-direction [Fig. 12(b)]. The effect of the injected current in the c-direction is different from that shown in Fig. 12 in that here, the critical current is unaffected by injection of 0.4 mA but suppressed by larger currents. This is not, however, evidence of spin–polarization and is again explicable entirely in terms of current addition. The critical current in this track was measured to be nonuniform, being 0.8 mA between contacts 7 and 9 and 1.2 mA between contacts 9 and 11 and, therefore, 0.8 mA between contacts 7 and 11, which were used when measuring spin-injection effects. The injection current flows to a common earth at contact 12 and not, therefore, through section 7-9. For $I_{\mathrm{inj}} < 0.4$ mA, the critical current of the track overall is therefore

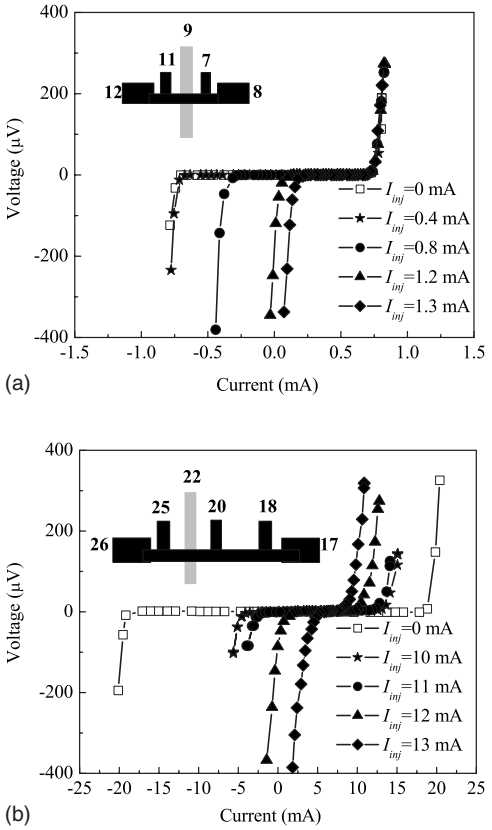

FIG. 12. Effect of current injection into sample 442 with a narrow crossover (a) for transport current in the c-direction (contact 12 is the common earth) and (b) for transport current in the a/b-direction (contact 26 is the common earth).

unaffected. As I_{inj} is increased above 0.4 mA, the critical current becomes limited by section 9-11, and hence, the transport current required to exceed the critical current on the negative current axis is reduced, while that on the positive axis is limited by section 7-9 and is therefore unaffected.

In the case of the a/b-axis track, we find that for $I_{\mathrm{inj}}=0$, the critical current is almost exactly the same when measured using voltage contacts 25-22, 22-20, and 20-18, implying that this track is rather uniform. We would expect to see effects very similar to those seen in Fig. 12(a) due to current summation in one or the other of the (now equal) regions either side of the crossover. We see that injection causes displacement in the negative current direction $>I_{\mathrm{inj}}$ *and* displacement in the positive current direction of opposite sign to that seen in Fig. 11. I_C has therefore been reduced, and to an extent which rapidly rises with I_{inj}, giving a gain $G=1.3$ at $I_{\mathrm{inj}}=13$ mA. This is a real suppression of the critical current and cannot be simply explained by current addition. It also implies that the suppression is taking place under the crossover and not in the tracks on either side as in Fig. 12(a). We see in Fig. 13 that a measurement of I_C without separate injection but using the crossover and the common ground for the transport current shows a current ~0.6 that obtained when measuring the critical current without injection in the normal way. These two observations would suggest that there is indeed suppression of I_C due to the polarization of I_{inj}. (We note in passing the symmetry with respect to the

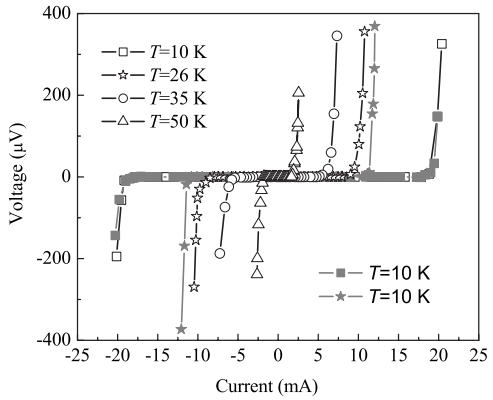

FIG. 13. V/I characteristics for the same sample (sample 442) shown in Fig. 12 for four different temperatures *without* an injection current. Also shown (solid stars) are data at 10 K, wherein the transport current was fed into the crossover rather than along the YBCO track.

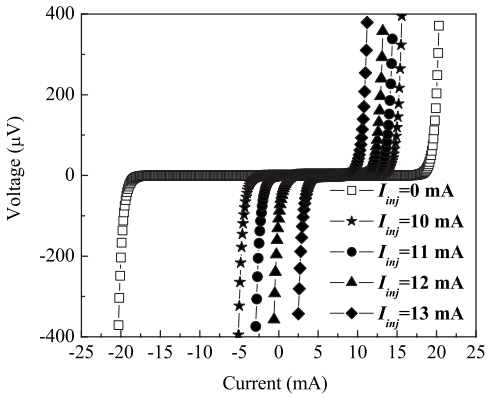

FIG. 14. Modeling of the data shown in Fig. 13(b) assuming a temperature rise due to heating and the effect of current summation under the crossover (see text for details).

direction of current injection when passing the transport current through the crossover. This provides no evidence in support of the suggestions[4] of a competitive effect between an equilibrium suppression by self-injection and spin-polarized injection from I_{inj}). We now offer two pieces of evidence *against* an interpretation of critical current suppression based on polarized spins.

(1) In Fig. 13, we show the V/I characteristics for the same sample with no injection at four different temperatures, together with a measurement at 10 K, wherein we passed the transport current through the crossover rather than along the YBCO track. We see that the suppressed I_C when passing the transport current through the crossover is consistent with heating to around 26 K, which we can attribute to the high injection current density in the narrow crossover through the measured 70 Ω contact resistance.

This cannot be a heating of the whole sample because the I_C measured between voltage contacts 20 and 18 is unaffected when the transport current is passed between 26 and 17 and 13 mA is injected into 22 (not shown). We are unaware of any measurements of thermal contact resistance between YBCO and a perovskite substrate at these temperatures, although measurements close to T_C give an approximate figure of 10^{-7} K W^{-1} m^2 (Ref. 32) implying a temperature rise under the crossover of 12 K. Thermal contact resistances involving insulating contacts are expected to increase with decreasing temperature (see Refs. 33 and 34 and references therein), so the required temperature rise of 16 K would not be unreasonable. In order to model the behavior in Fig. 12(b), we must therefore allow for the combined effects of both heating and current summations under the crossover. We first assume that the V/I characteristics of the YBCO track are given by a simple exponential behavior, $V=A\exp\{[I-I_C(0)]/f(T)\}$, where A is a constant and $I_C(0)$ is the zero temperature critical current. This is a considerable simplification for the current voltage dependence. It does, however, explain why all our V/I curves at a given temperature have a similar slope at the same detection voltage even when measured over very different lengths of track since the behavior is very strongly dominated by the exponential term. This point does not seem to have been noted in other works in this area. The temperature dependence $f(T)$ is clearly much less strong than linear, as evidenced by the similar slopes shown in Fig. 13, so we have taken it as a constant f. We have determined A, I_C, and f by fitting to the $I_{\mathrm{inj}}=0$ data at 10 K. We know the amount of heating caused by passing 13 mA through the crossover and we assume that this heating is proportional to I_{inj}^2. The dependence of I_C on temperature is obtained from Fig. 13. Finally, In calculating the effect of current summation, we assume that the injection current uniformly enters through the crossover.

The results of our modeling are shown in Fig. 14. The fit to Fig. 12(b) is not perfect, but given the great simplicity of our model, we see no reason to assume that spin–polarization is necessary to explain our results.

We should emphasize that it is not an aim of this work to explain the detailed nature of the V/I characteristics in terms of flux flow in the self-field limit, and our measurements are insufficiently detailed to do this with any confidence. The simple exponential dependence assumed here is most safely simply taken as a convenient equation for fitting our data and interpreting the effects of the injection current.

(2) We would expect that, if the observed gain were due to spin–polarization, we might see effects due to the application of a magnetic field sufficient to take the sample around a hysteresis loop of the LCMO for the reasons discussed in Sec. I. The importance of magnetic field measurements in deconvolving spin-injection effects from other processes was emphasized in Ref. 12. We have applied magnetic fields up to 150 mT both in the plane and perpendicular to the plane of the film. This suppresses J_C by about 20% in the same way as for our films with no LCMO layer, but we find no difference in the effect of I_{inj} with and without the field.

In summary, therefore, we believe that the $G>1$ observed in our samples is entirely explicable in terms of heating below the crossover combined with current summation in the same area.

If we assume that our injected current is uniform, then our maximum injection current density is 1.5×10^6 A m^{-2} for the wide crossover and 1.3×10^8 A m^{-2} for the narrow crossover. These are comparable with, or higher than, injection current densities reported in the literature and for which gain

>1 was claimed (e.g., Ref. 10 reported a gain of 35 with 10^5 A m^{-2} injection current density into *c*-axis perpendicular-to-plane YBCO films).

We cannot deduce from our experiments that polarized spins have no effect on *c*-axis in-plane YBCO. Indeed, it would be surprising if there was no effect at some level. However, any such effects must be below our detection level. Our HRTEM measurements show a very high degree of epitaxy at the interfaces, and our EDX data suggest that there is no diffusion of cations across the interface to within our resolution of 10 nm. Manganese ions, however, are a particular worry because they are magnetic in all their valence states, and a layer of randomly oriented manganese ions near the interface could seriously disorientate the spin-polarized nature of the injected current, as indeed could charges at the interface, via spin-orbit scattering. We cannot therefore rule out the possibility that specimens with higher quality interfaces would show significant effects.

IV. CONCLUSIONS

We have made detailed measurements of the effect of an LCMO layer on the properties of *c*-axis in-plane YBCO films in order to investigate the effect of contact with the *a*/*b*-plane of the YBCO. In the equilibrium state of the YBCO, which was probed by penetration depth measurements, we find effects that are the opposite of those expected for suppression of superconductivity by the spin–polarization in the LCMO and which are explicable in terms of direct suppression of superconductivity by a magnetic field. In the case of current injection, we find suppression of the critical current of the YBCO, but this is explicable by the combined effects of heating and current summations. We therefore find no evidence that spin–polarization suppresses superconductivity in *c*-axis in-plane YBCO films for tracks patterned along either the *a*/*b* or *c*-direction.

*Present address: Department of Physics, University of Puerto Rico, San Juan, Puerto Rico 00931-3343, USA.
†Present address: Department of Physics, University of Turku, Turku FIN-20014, Finland.

[1] S. Horwitz, D. Koller, M. S. Osofsky, R. J. Soulen, and R. C. Auyeung, J. Appl. Phys. **83**, 7189 (1998).
[2] V. A. Vas'ko, V. A. Larkin, P. A. Kraus, K. R. Nikolaev, D. E. Grupp, C. A. Nordman, and A. M. Goldman, Phys. Rev. Lett. **78**, 1134 (1997).
[3] Z. W. Dong, R. P. Ramesh, T. Venkatesan, M. Johnson, Z. Y. Chen, S. P. Pai, V. Talyansky, R. P. Sharma, R. Shreekala, C. J. Lobb, and R. L. Greene, Appl. Phys. Lett. **71**, 1718 (1997).
[4] N. C. Yeh, R. P. Vasquez, C. C. Fu, A. V. Samoilov, Y. Li, and K. Vakili, Phys. Rev. B **60**, 10522 (1999).
[5] D. Koller, M. S. Osofsky, D. B. Chrisey, J. S. Horwitz, R. J. Soulen, R. M. Stroud, C. R. Eddy, J. Kim, R. C. Y. Auyeung, J. M. Byers, B. F. Woodfield, G. M. Daly, T. W. Clinton, and M. Johnson, J. Appl. Phys. **83**, 6774 (1998).
[6] A. M. Goldman, P. I. Kraus, K. Nikolaev, V. Vas'ko, A. Bhattacharya and W. Cooley, J. Supercond. **14**, 283 (2001).
[7] S. Bhattacharjee and M. Sardar, Phys. Rev. B **62**, R6139 (2000).
[8] S. Sarkar, P. Raychaudhuri, P. K. Mal, A. R. Bhangale, and R. Pinto, J. Appl. Phys. **89**, 7502 (2001).
[9] R. J. Kinsey, G. Burnell, and M. G. Blamire, IEEE Trans. Appl. Supercond. **11**, 904 (2001).
[10] R. M. Stroud, J. Kim, C. R. Eddy, D. B. Chrisey, J. S. Horwitz, D. Koller, M. S. Osofsky, R. J. Soulen, and R. C. Auyeung, J. Appl. Phys. **83**, 7189 (1998).
[11] K. Lee, W. Wang, L. Iguchi, B. Friedman, T. Ishibashi, and K. Sato, Appl. Phys. Lett. **75**, 1149 (1999).
[12] Y. Gim, A. W. Kleinsasser, and J. B. Barner, J. Appl. Phys. **90**, 4063 (2001).
[13] H. L. Zhao and S. Hershfield, Phys. Rev. B **52**, 3632 (1995).
[14] Q. Si, Phys. Rev. Lett. **78**, 1767 (1997).
[15] P. Mikheenko, M. S. Colclough, C. Severac, R. Chakalov, F. Wellhoffer, and C. M. Muirhead, Appl. Phys. Lett. **78**, 356 (2001).
[16] A. V. Sergeev, A. D. Sevenov, P. Kouminov, V. Trifonov, I. G. Goghidze, B. S. Karasik, G. N. Goltsmans, and E. M. Gershenzon, Phys. Rev. B **49**, 9091 (1994).
[17] M. D. Allsworth, R. Chakalov, M. S. Colclough, P. Mikheenko, and C. M. Muirhead, Appl. Phys. Lett. **80**, 4196 (2002).
[18] M. D. Alsworth, R. A. Chakalov, P. Mikheenko, M. S. Colclough, and C. M. Muirhead, IEEE Trans. Appl. Supercond. **13**, 2849 (2003).
[19] V. Pena, Z. Sefrioui, D. Arias, C. Leon, J. Santamaria, J. L. Martinez, S. G. E. te Velthuis, and A. Hoffman, Phys. Rev. Lett. **94**, 057002 (2005).
[20] G. X. Miao, K. S. Yoon, T. S. Santos, and J. S. Moodera, Phys. Rev. Lett. **98**, 267001 (2007).
[21] C. Bell, S. Tursucu, and J. Aarts, Phys. Rev. B **74**, 214520 (2006).
[22] S. Poelders, R. Auer, G. Linker, R. Smithey, and R. Schneider, Physica C **247**, 309 (1995).
[23] I. E. Trofimov, A. P. Litvinchuk, K. Kamaras, C. Thomsen, and H.-U. Habermeier, J. Supercond. **7**, 209 (1994).
[24] R. Ramesh, C. C. Chang, T. S. Ravi, D. M. Hwang, A. Inam, X. X. Xi, Q. Li, X. D. Wu, and T. Venkatesan, Appl. Phys. Lett. **57**, 1064 (1990).
[25] R. J. Cava, B. Batlogg, C. H. Chen, E. A. Rietman, S. M. Zahurak, and D. Werder, Phys. Rev. B **36**, 5719 (1987).
[26] D. Jorgensen, B. W. Veal, A. P. Paulikas, L. J. Nowicki, G. W. Crabtree, H. Claus, and W. K. Kwok, Phys. Rev. B **41**, 1863 (1990).
[27] R. A. Chakalov, G. Passerieux, I. P. Jones, P. Mikheenko, J. Ireland, R. I. Chakalova, M. S. Colclough, and C. M. Muirhead, J. Appl. Phys. **98**, 123908 (2005).
[28] M. Tinkham, *Introduction to Superconductity* (Dover, New York 1996).
[29] N. D. Mathur, H.-H. Jo, J. E. Evetts, and M. G. Blamire, J. Appl. Phys. **89**, 3388 (2001).
[30] I. S. Burmistrov and N. M. Chtchelkatchev, Phys. Rev. B **72**, 144520 (2005).
[31] M. Covington, R. Scheuerer, K. Bloom, and L. H. Greene, Appl.

Phys. Lett. **68**, 1717 (1996).
[32] Yu. M. Bouguslavskij, K. Joosse, A. G. Sivakov, F. Roesthuis, G. J. Gerritsma, and H. Rogalla, Physica C **220**, 195 (1994).
[33] R. E. Peterson and A. C. Anderson, J. Low Temp. Phys. **11**, 639 (1973).
[34] R. S. Prasher and P. E. Phelan, J. Low Temp. Phys. **10**, 473 (1997).